Atmospheric Environment 196 (2019) 164–178

Contents lists available at ScienceDirect

Atmospheric Environment

journal homepage: www.elsevier.com/locate/atmosenv

Synoptic and local circulations associated with events of high particulate pollution in Valparaiso, Chile

Diana Pozo[a,d], Julio C. Marín[a,d], Graciela B. Raga[b,*], Jorge Arévalo[a,e], Darrel Baumgardner[c], Ana M. Córdova[a], Jorge Mora[a]

[a] Departamento de Meteorología, Universidad de Valparaíso, Chile
[b] Centro de Ciencias de la Atmósfera, Universidad Nacional Autónoma de México, Mexico
[c] Droplet Measurements Technology, USA
[d] Centro de Estudios Atmosféricos y Astroestadística, Universidad de Valparaíso, Chile
[e] Department of Hydrology and Atmospheric Sciences, University of Arizona, Tucson, USA

ARTICLE INFO

Keywords:
Pollution episodes
Black carbon
Synoptic forcing
Land-sea breeze

ABSTRACT

This study discusses the synoptic situations associated with cases of high pollution in terms of black carbon (BC) concentrations observed at the research site during the four months of the VAMPIRE campaign that is described fully in the companion study by Marín et al. (2017). Cases in which the concentration of BC exceeded the 85th percentile were selected to evaluate composite synoptic situations, resulting in a total of fifteen cases analyzed. These fifteen cases occurred during one of the three prevalent synoptic situations identified and labeled as: i) ***Coastal low***, characterized by weak easterly winds and low planetary boundary layer (PBL) height due to an enhancement of the temperature inversion before the arrival of the coastal low; ii) ***Pre-frontal***, also characterized by low PBL height, with a cold front approaching from the South and the coastal low retreating northwards, also associated with pollution episodes in Santiago (Rutllant and Garreaud, 1995); and iii) ***SEP anticyclone*** characterized by large stability, very low gradient in the mean sea level pressure and weak westerly-southwesterly wind due to the dominance of the southeast Pacific anticyclone. ***Coastal low*** cases were observed not only during winter but also in all four months of the VAMPIRE field campaign, while ***Pre-frontal*** cases were observed only at the end of July and August 2014. All three synoptic situations are consistent with a reduced synoptic forcing, in which the mesoscale sea-land breeze predominates and advects large pollutant concentrations from local/regional emission sources to the research site. Detailed analysis is presented here for two case studies: one ***Coastal low*** and one ***Pre-frontal***, combining the observations of pollutants as well as mesoscale modeling with the WRF model to estimate back-trajectories and evaluate the relative role of the synoptic and mesoscale forcing on the pollution episodes in Valparaiso. These synoptic conditions and their interplay with meso-scale circulations identified during VAMPIRE provide evidence and insight that will aid in future air quality forecasts for Valparaiso.

1. Introduction

Many studies have shown the strong impact that meteorological conditions have on the formation, dispersal, and removal of pollution in the atmosphere (Hidy et al., 1978; Bei et al., 2012, 2013; Wu et al., 2013; Wang et al., 2014). Specifically, a large number of investigations have identified the large-scale synoptic patterns related to events of high pollution. High pollution levels have been often linked with high pressure synoptic systems, stable air, shallow planetary boundary layers (PBL) and weak winds. Davis and Kalkstein (1990) found high concentrations of pollution in the US during stable air under anticyclonic conditions. Wei et al. (2011) determined that coarse particulate (PM_{10}) accumulation in northern China occurred under the direct influence of the center of an anticyclonic system. Bei et al. (2016) identified four synoptic conditions as favorable for high fine particulate ($PM_{2.5}$) concentrations in the Guanzhong basin in China during wintertime; the presence of a high-pressure system inland was most frequently associated with high levels of $PM_{2.5}$. Hamburger et al. (2011) concluded that an anticyclonic blocking event favored the increase in pollution concentrations over central Europe. In the Sydney basin, Australia, Crawford et al. (2016) found that high pressure systems were related to elevated $PM_{2.5}$ concentrations. Cheng et al. (2008) found that high

* Corresponding author. Centro de Ciencias de la Atmósfera Universidad Nacional Autónoma de México, Mexico.
E-mail addresses: raga.graciela@gmail.com, raga@unam.mx (G.B. Raga).

https://doi.org/10.1016/j.atmosenv.2018.10.006
Received 4 February 2018; Received in revised form 2 October 2018; Accepted 7 October 2018
Available online 10 October 2018
1352-2310/

pressure and the approach of a front were both associated with high levels of pollution in northern China and Wu et al. (2013) found that poor air quality over the Pearl River Delta was associated with pre-cold front conditions, as well as during tropical cyclone conditions.

Mesoscale circulations can also have a strong impact on air quality, particularly in coastal cities or within lake basins. Studies on the effect of sea- or lake-breeze on the transport of pollution typically rely on the use of a mesoscale atmospheric model and a trajectory model (Eastman et al., 1995; Harris and Kotamarthi, 2005; Crawford et al., 2016; Jiang et al., 2016). Eastman et al. (1995) and Harris and Kotamarthi (2005) determined that the time and extension of inland penetration of the lake-breeze is a key factor in the transport of pollutants and its re-circulation. Jiang et al. (2016) pointed out the importance of the interaction between mesoscale and synoptic scale circulations that favored elevated ozone (O_3) and $PM_{2.5}$ concentrations in the Sydney bay basin.

Previous research on air quality in Chile has focused primarily on its capital and largest city, Santiago, which suffers from very high particulate pollution, mainly during winter. More recently, other selected southern cities (e.g. Osorno, Rancagua, Temuco) with serious particulate concentrations have also been studied. In particular, some studies have analyzed the relation between pollution and meteorological factors. Garreaud and Rutllant (2006) (book chapter in Spanish) described the role of the basin-wide circulation in Santiago on local pollution. Gramsch et al. (2014) observed that $PM_{2.5}$ and black carbon concentrations were higher in several parts of Chile on days with near-surface temperature inversions. Yañez et al. (2017) used statistical methods to show that particulate matter in different inland cities of Chile is largely related to meteorological variables, highlighting their importance as air quality forecasting tools. Moisan et al. (2017) developed a forecasting method based on dynamic multiple equations to predict $PM_{2.5}$ in Santiago. Saide et al. (2016) and Cuchiara et al. (2017) used the Weather Research and Forecasting model with its Chemistry module (WRF-Chem) as a successful method to forecast air quality in Santiago and other inland cities in Chile.

Despite the number of air quality studies performed in Chile, only a few of them have analyzed the impact of synoptic and mesoscale circulations on pollution levels. Rutllant and Garreaud (1995) showed that high pollution events in Santiago between April and August (austral fall and winter) were primarily related to two synoptic situations off-shore of central Chile: i) the onset of a surface coastal low (as the most frequent event), and ii) its demise, in which a cold front approaches from the south. Both situations enhance subsidence and decrease the planetary boundary layer (PBL) height. More recent studies have evaluated the impact of regional circulations on the transport of pollution up to the Andean cryosphere (Orfanoz-Cheuquelaf et al., 2015; Cordova et al., 2016; Huneeus et al., 2016).

Black carbon (BC) is a component of $PM_{2.5}$ that is emitted primarily from anthropogenic sources. Numerous studies have also recognized the negative effects of BC on human health since it can worsen respiratory and cardiovascular conditions, and cause even mortality (Janssen et al., 2011, 2012; Hoek et al., 2013; Grahame et al., 2014). In addition, BC directly impacts climate from the net heating of the atmosphere by the absorption of solar radiation. BC can also reduce the albedo or even enhance the melting of ice and snow-covered surfaces (Ramanathan and Carmichael, 2008; Bond et al., 2013; Ménégoz et al., 2014). Furthermore, BC may act as cloud condensation or ice nuclei, indirectly affecting clouds and the climate system (Bond et al., 2013; Jiang et al., 2013).

The current study focuses on the city of Valparaiso, a subtropical coastal city in central Chile, characterized by a complex topography with steep hillsides that circle the bay, which is the largest commercial port in Chile as well as the main Navy base. Few studies have been conducted in Valparaiso and neighboring areas to quantify pollution and/or the impact of local and regional circulations on air quality. Olivares et al. (2002) suggested that the city can be impacted during episodic events by sulfur plumes that come from the Ventanas industrial zone located to the north. Toro et al. (2013) and Seguel et al. (2013) report on measurements of surface O_3 and its precursors in different cities of central Chile in March and April 2010 and concluded that O_3 can be transported over large distances across central Chile.

The Valparaiso Atmospheric Measurements of Pollution and Impact on the Regional Environment (VAMPIRE) field campaign was a collaborative project between the University of Valparaiso (UV) and the Universidad Nacional Autónoma de Mexico (UNAM) to measure, for the first time, certain optical, chemical and physical properties of aerosol particles that are relevant for air quality, radiative transfer and meteorology. A fairly large instrumentation suite was deployed in this port city, as detailed in Marín et al. (2017). VAMPIRE took place over four different periods: i) 25 July - 25 August 2014 (August 2014, from here forward); ii) December 2014; iii) January 2015, and iv) March 2015. Marín et al. (2017) focused on the characterization of daily and seasonal behavior of BC in Valparaíso city and the identification of its sources. The work reported in this study fully describes the meteorological conditions and the synoptic and/or local circulations that are related to the selected high pollution episodes with large BC concentrations.

We begin by describing the general climate and meteorology of Valparaiso followed by a brief review of the instruments used to measure the local meteorological conditions and aerosol properties. Composites of atmospheric fields of the identified cases of high pollution (in terms of BC concentrations) are described in detail and two cases are selected for further analysis. A high-resolution mesoscale simulation is then employed to evaluate the synoptic and mesoscale circulations that are linked to episodes of high BC.

2. Climate and meteorology of Valparaiso

Valparaíso, characterized by a generally mild climate, is located in a transition region between the dry and hot conditions of northern Chile and the humid and cold conditions of southern Chile. The region is under the influence of the permanent subtropical Southeast Pacific (SEP) anticyclone (Rodwell and Hoskins, 2001; Barrett and Hameed, 2017). At low levels and between 10 and 35 S, southerly winds are induced along the coast of Chile by the SEP anticyclone's circulation, which causes the advection of colder waters from the South and the upwelling of deeper cold waters due to the wind stress on the sea surface. In addition, the cold Humboldt current flows northward along the Chilean coast. Warm and dry conditions aloft due to adiabatic compression, and cold and moist conditions in the marine boundary layer generate a thermal inversion, typically located below 1 km, that is usually capped by stratus clouds (Bretherton et al., 2004; Comstock et al., 2005; Hannay et al., 2009; Muñoz and Undurraga, 2010). Deep convection cannot develop over the ocean or the continent due to this pervasive thermal inversion and, in conjunction with steep mountains slopes along the coast, the flow of humid air inland is blocked (Rutllant et al., 2003).

Most of the precipitation in Valparaiso is associated with the passage of frontal systems during winter with cutoff lows affecting the region also contributing to total rainfall (Pizarro and Montecinos, 2000). Large-scale factors such as the El Niño Southern Oscillation (ENSO) and the SEP anticyclone on interannual (Rutllant and Fuenzalida, 1991; Montecinos and Aceituno, 2003) and seasonal scales (Barrett and Hameed, 2017) modulate precipitation. Another synoptic situation that may affect Valparaiso was identified by Garreaud et al. (2002) as an off-shore area of lower surface pressure observed frequently during austral winter and spring, who labeled it “coastal low”. The outskirts of the SEP anticyclone and the continent flank this tongue-shaped area of low pressure. This coastal low can lead to episodes of low-level stratocumulus and fog in Valparaiso. Typically dry conditions and hot temperatures predominate in summer, but fog and stratocumulus clouds can also be present.

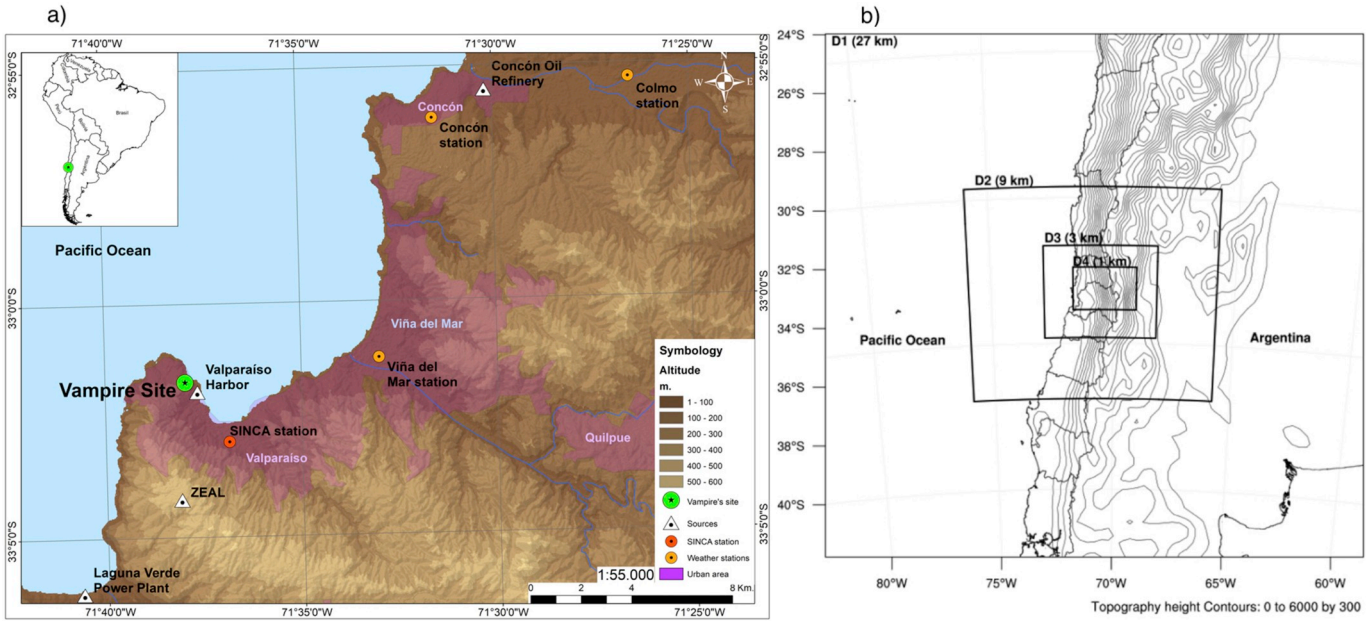

Fig. 1. a) Google Earth view of South America and a zoom-in showing the location of the city of Valparaiso, its bay, the research site (green circle), the surrounding pollution sources described in the text (triangles), the atmospheric weather stations used for model validation (orange circles) and the official SINCA air-quality station at downtown Valparaiso (red circle), b) four-nested domains configuration used in the WRF simulations. (For interpretation of the references to color in this figure legend, the reader is referred to the Web version of this article.)

3. Observations

3.1. Field campaign

The VAMPIRE field campaign was conducted on the terrace of the Meteorology Department of the University of Valparaiso (33.028264°S, 71.633140°W, 68m amsl). Fig. 1a shows the location of the city of Valparaíso and its protected bay, as well as the research site (green circle), the official SINCA monitoring station (red circle), the atmospheric weather stations used to validate the regional simulations (orange circles) and a few of the major nearby pollution sources (ZEAL, the Concon oil refinery, and the thermoelectric power plant in Laguna Verde). The inset shows Valparaiso within the context of South America.

The instruments used during VAMPIRE to sample the physical, chemical and optical properties of aerosol particles are fully described in Marín et al. (2017) and we refer to it for details of the instrumentation, corrections applied and for the sampling and analysis strategies. Only the description of the estimate of equivalent black carbon (eBC) is included here. The eBC is derived from the absorption coefficient, B_{abs}, that is measured with a Photoacoustic Extinctiometer (PAX). The photoacoustic technique converts the pressure waves, created by the heating of black carbon particles that absorb light at 870 nm, into B_{abs}. The conversion factor is determined by calibration through a two-step process that introduces high concentrations of purely light-scattering particles followed by high concentrations of partially absorbing particles to the measurement cells (Arnott et al., 2000; Nakayama et al., 2015). The conversion of B_{abs} to eBC is with a mass specific absorption cross section of 4.74 m^2g^{-1}. The uncertainty in B_{scat} is approximately ± 10% due to the accuracy of calibration, truncation errors and aerodynamic losses in the inlet to the sample cavity. The uncertainty in B_{abs} is approximately ± 20%, from the accuracy of calibration and inlet losses. Given the range and uncertainty in the mass-specific absorption cross section, the derived eBC mass concentrations have an uncertainty that could be as large as 55–60% but is on average closer to 30%. For greater detail on the PAX, the interested reader is directed to the study by Retama et al. (2015). In the context of this study we only present time series of eBC and fine particulate mass concentration ($PM_{2.5}$) for two selected case studies described in Section 5.2.

A VAISALA CL-31 ceilometer was used to determine the vertical profiles of aerosol backscatter at a wavelength of 910 nm. This instrument in essence functions as a light detection and ranging (LIDAR) sensor, providing measurements from 20m to 7 km above ground level, with a 20m vertical resolution. The ceilometer-derived vertical profile of aerosol backscatter is useful to determine the boundary layer height and structure (Mü;nkel et al., 2007; van der Kamp and McKendry, 2010; Tsaknakis et al., 2011; Garcia-Franco et al., 2018). Even though the instrument measurement frequency is 0.5Hz, the raw data were averaged every 10 min. The accuracy of the vertical profile is ± 5m. In order to translate the raw backscattered power (unitless) to units of backscattered extinction the following procedure, described in Raga et al. (2013) is applied. The in-situ extinction coefficient derived from the PAX is correlated with the low-level (between 20 and 60 m) for selected periods when the surface layer was considered well-mixed and there was no fog. A linear fit between these independent measurements is obtained, forcing the fit through zero, which provides the conversion from raw backscattered power to extinction coefficient as a function of height. The correlation coefficient between the raw backscatter and extinction coefficient derived from the PAX was > 0.9 with a statistical uncertainty of $P < 0.001$. The best fit line, going through the zero was 0.553 raw ± 0.004.

A simple algorithm that determined the boundary layer height from the sharp gradient of the extinction coefficient was developed (following Münkel et al., 2007) and provided an adequate estimate, when compared with manual inspection. Nevertheless, the large variability seen in conditions at the research site throughout the different months of measurements, due sometimes to the presence of low-level fog, made it difficult for the automated algorithm to correctly determine the boundary layer height from the ceilometer.

3.2. SINCA monitoring and radiosonde stations

The $PM_{2.5}$ data from three National System for Air Quality (SINCA in Spanish) monitoring stations were used in this study: the one located in downtown Valparaiso (33.04962°S, 71.61372°W and 20m amsl), and two others located in the capital city of Santiago at Parque O'Higgins (70.6607°W, 33.4642°S) and Las Condes (70.5233°W, 33.3768°S). The $PM_{2.5}$ measurements are made using the beta-attenuation technique (Thermo, Model 5014i).

Radiosondes are launched daily or twice daily at 00 and 12 UTC -corresponding to 20 and 08 local time (LT), respectively-at Santo Domingo, a small coastal town located 95 km south of Valparaiso, at 33.7°S, 71.6°W. This is one of the four sites in Chile where radiosondes are launched by Chilean meteorological weather service personnel. Measurements include temperature, humidity, pressure, height, wind speed and direction, as the balloon with the attached sensors ascends through the atmosphere. Radiosonde data from station Santo Domingo (code 85586 SCSN) were downloaded from the website: http://weather.uwyo.edu/upperair/sounding.html, and the data were plotted in Skew-T diagrams for selected case studies.

3.3. Industrial emissions in/near Valparaiso

In 2011, the Chilean authorities released an emissions inventory for the region of Valparaiso (Valparaiso Emissions inventory, 2011). According to this database, the main sources of $PM_{2.5}$ in the region are two thermoelectric plants, which combined emit about 2465.83 tons/year. The one located at Laguna Verde emits the highest amount of $PM_{2.5}$, followed by the one located at the Concón-Ventanas industrial park. Other important sectors with emissions of $PM_{2.5}$ are the fuel production and storage (1454.03 tons/year) and copper production (1073.47 tons/year), also located at the Concón-Ventanas industrial park.

Thermoelectric plants at Laguna Verde and Concón-Ventanas are also the main emission sources of carbon monoxide (CO), with values of 1454.03 tons/year and 1073.47 tons/year, respectively. The highest emission rates of sulfur dioxide (SO_2) in the region are associated with primary copper production in Concón-Ventanas (33015.89 tons/year) and thermoelectric plants (15587.29 tons/year), which use coal as fuel.

4. Climate Forecast System Reanalysis and the WRF model

Version 2 of the Climate Forecast System (CFSv2, Saha et al., 2014), run by the National Centers for Environmental Prediction (NCEP), was created for the purpose of extending the Climate Forecast System Reanalysis (CFSR) from 1 January 2011 until present. This dataset was used to identify the synoptic conditions associated with periods of high concentrations of BC during the VAMPIRE field campaign. Composite maps of mean sea level pressure, geopotential height, static stability parameter (S), relative vorticity and wind fields at low- and mid-levels in the atmosphere were analyzed during the four months of VAMPIRE. In addition, we analyzed the synoptic situation for selected cases during August 2014, one of the months with the highest concentrations of BC recorded at the field site. The static stability parameter at 850 hPa was defined as:

$$S = \frac{T}{\theta} \cdot \frac{\partial \theta}{\partial p}$$

where T and θ are the temperature and potential temperature at 850 hPa, respectively, and the partial potential temperature derivative with pressure was calculated using data between 1000 hPa and 850 hPa.

The Weather Research and Forecasting (WRF) model is a numerical weather prediction system freely available that can be used for operational and research purposes (Skamarock et al., 2008). A high-resolution simulation was performed with Version 3.6.1 of the Advanced Research WRF core (ARW-WRF). Four nested domains were employed in the simulation as depicted in Fig. 1b. Results from the smallest domain (domain 4, D4), with the highest horizontal resolution (1 km), were analyzed for this study. The simulation employed the land-use data based on the Moderate Resolution Imaging Spectroradiometer (MODIS) land-cover classification of the International Geosphere-Biosphere Programme and modified for the National Oceanic and Atmospheric Administration (NOAA) land surface model at 30 arc seconds (approximately 0.9 km) in horizontal resolution.

The simulation included 60 vertical levels at variable resolution, with eight levels within the first kilometer and spacing varying between 60 and 200 m. The simulation was performed for the period 25 July to 15 October 2014, but only two selected cases were analyzed and presented here. Output from the simulation were saved every hour. The CFSv2 provided the initial and boundary conditions every 6 h, and an analysis nudging was implemented in the outer domain (D1) to provide better boundary conditions during the simulation period. A more detailed description of the WRF configuration and domains can be found in Cordova et al. (2016). We discuss here in detail the results of the WRF simulation for two high-pollution events, as determined by BC concentrations: 31 July 2014 and 13 August 2014.

The planetary boundary layer (PBL) height was estimated by the WRF model to analyze the evolution of the boundary layer during the two high-pollution cases discussed in Section 5.2. The WRF simulations used the PBL parameterization of Mellor-Yamada-Nakanishi-Niino Level 2.5 (Nakanishi and Niino, 2004, 2006), which is a one and a half order prognostic turbulent kinetic energy (TKE) scheme with local vertical mixing. This scheme improves the underestimation of TKE and the insufficient growth of the convective boundary layer present in the Mellor-Yamada scheme by using a database of large eddy simulations. The estimated PBL height is defined as the height at which the TKE is less than a critical value ($1.0 \times 10^{-6}\,m^2\,s^{-2}$).

The output for the WRF model simulation was compared with observations at surface weather stations during the period 25 July to 31 August 2014 (first intensive period of measurements in VAMPIRE campaign) in order to validate the model performance during this study. We used the weather station installed at the research field site and three other weather stations (Viña del Mar, hereafter VM, Colmo and Concón) located inside the innermost domain in the model. Note that not all variables were available from all four weather stations to compare with the model.

Figure S1 and Table S1 in the supplementary material (SM) show that the near-surface temperature is overestimated by the model in VAMPIRE and VM stations with an rmse of 3.6 °C and 4.1 °C, respectively. The mean bias was below 1.6 °C in both station for August 2014, although it can be much larger during specific periods (see case study below). Mean absolute biases between 0.32 °C and 2.5 °C were reported in 3-day WRF forecasts by Saide et al. (2016) using the same version of the model in the comparison of nine stations. The near-surface relative humidity (RH) is mainly underestimated by the model in VAMPIRE and VM stations, with an rmse larger than 20%. Nevertheless, the model represents reasonably well the temperature and relative humidity variability during the period, showing correlation coefficients between 0.6 and 0.7 at those stations. As a comparison, Saide et al. (2016) show values for temperature between 0.7 and 0.91 for all stations. Figure S1 indicates that the model exhibits a hot and dry bias during daytime. This is possibly related to a misrepresentation of the low-level cloudiness that usually arrives from the ocean and covers the city, as will be discussed below in the analysis of one of the high-pollution study cases.

The surface pressure at the VM station is very well represented by the model, showing an rmse of 2 hPa and a correlation coefficient of 0.9. Figure S1 shows that the model represents reasonably well the wind speed variability at the VAMPIRE station and at the other stations (not shown). However, the model largely overestimates the maximum wind speeds and underestimates several episodes of weak winds ($\sim 1\,ms^{-1}$) that occur on several days during August 2014. This, in addition to the complex topography of the region makes it difficult for

the model to accurately simulate wind speed. In spite of that, most of the time the u- and v-components of the wind show a reasonable correlation coefficient (0.5–0.6) during the campaign. Saide et al. (2016) obtained comparable values (between 0.5 and 0.9) for the comparison of simulated wind speed. They mention that the smallest values were observed for stations in central Chile when wind speeds were generally low. Winds at the research site were also low most of the time during August 2014, affecting the ability of the model to accurately represent them. Overall, the performance of the model is good and comparable to the results obtained by the simulations reported by Saide et al. (2016) for stations in Chile. The performance of the model representing near-surface variables and the evolution of the PBL height during two high-pollution cases is discussed below.

5. Results and discussion

5.1. Composite synoptic conditions during high BC episodes

The eBC concentrations observed during the VAMPIRE campaign were larger in August 2014 and March 2015 than in December 2014 and January 2015 (see Fig. 3 in the companion paper by Marín et al., 2017). Periods of high eBC concentrations were found to be associated with three distinct synoptic situations. The first was characterized by weak easterly winds and low PBL height, due to an enhancement of the temperature inversion before the arrival of the coastal low. This is the most typical synoptic situation found by Rutllant and Garreaud (1995) to be associated with severe pollution episodes in Santiago during winter months. We note that this situation was observed not only during winter but also in all four months of the VAMPIRE field campaign. The second synoptic situation also shows low PBL heights and corresponds to the case of a cold front approaching from the South and the coastal low retreating to the North. The cyclonic circulations associated with the surface low and the coastal low, and the circulation associated with the SEP anticyclone result in slow and divergent surface winds in the region. Rutllant and Garreaud (1995) mentioned that this less frequent situation was also associated with pollution episodes in Santiago. This pre-frontal situation was observed during VAMPIRE only at the end of July and August 2014 since cold fronts affect the region mostly in the austral winter. The third synoptic situation associated with high eBC concentrations occurred with the prevalence of stable conditions and calm winds near the surface, with a very low gradient in the mean sea level pressure over Valparaíso and nearby areas, and a strong presence of the SEP anticyclone.

All three situations are consistent with a reduced synoptic forcing during which the mesoscale sea-land breeze may become predominant, likely advecting large pollutant concentrations from local/regional emission sources to the field site. Furthermore, the reduced PBL height and calm winds associated with these synoptic situations can lead to the quite high eBC concentrations that were measured. At times, the eBC concentrations measured were even comparable to values observed in megacities like Mexico City (Retama et al., 2015).

Composite synoptic maps were constructed for a number of episodes of high eBC concentrations, for each of the three synoptic situations described above, to the nearest hour. Only episodes with eBC concentrations higher than the monthly 85th percentile (computed for each of the months of the project) and lasting at least 6 h, were selected for the composites. Table 1 shows the date and number of hours of selected cases with eBC concentrations > 85th percentile, the observed averaged eBC and $PM_{2.5}$ values and the synoptic situation present during the episode. Seven high eBC episodes following the above criteria occurred during the four months of VAMPIRE field campaign, in which the coastal low approached Valparaiso from the North (labeled ***Coastal low*** in Table 1), three cases were associated with pre-frontal synoptic situations between the end of July and August 2014 in which the coastal low was retreating northwards (labeled ***Pre-frontal*** in Table 1), and five episodes were observed when stable conditions and weak westerly winds were present under almost constant mean sea level pressures (labeled ***SEP anticyclone*** in Table 1).

Table 1
Day and number of hours, averaged $PM_{2.5}$ and eBC concentrations, and the synoptic situation present during the events of eBC concentrations larger than the 85th percentile for each month during VAMPIRE. Rows in bold identify the days discussed in detail as case studies.

Day [time UTC]	$PM_{2.5}$ [μg/m^3]	eBC [μg/m^3]	Synoptic situation
29 July 2014 [18, 24]	19.7	5.9	*SEP anticyclone*
31 July 2014 [6, 12, 18, 24]	**26.8**	**6.6**	***Pre-frontal***
4 August 2014 [12, 18, 24]	23.4	3.2	*Pre-frontal*
13 August 2014 [12, 18, 24]	**14.4**	**4.5**	***Coastal low***
16 August 2014 [6, 12]	17.6	6.5	*Pre-frontal*
3 Dec. 2014 [6, 12, 18, 24]	8.4	2.5	*Coastal low*
4 Dec. 2014 [6, 12, 18]	11.0	3.8	*SEP anticyclone*
11 Dec. 2014 [12, 18]	8.2	3.9	*SEP anticyclone*
12 Dec. 2014 [6, 12, 18]	11.4	3.0	*Coastal low*
3 January 2015 [6, 12]	9.0	2.5	*Coastal low*
8 January 2015 [6, 12]	16.8	3.6	*Coastal low*
13 January 2015 [6, 12]	12.7	3.0	*SEP anticyclone*
29 January 2015 [6, 12]	13.3	3.0	*SEP anticyclone*
13 March 2015 [6, 12]	21.3	5.2	*Coastal low*
15 March 2015 [6, 12]	22.8	7.7	*Coastal low*

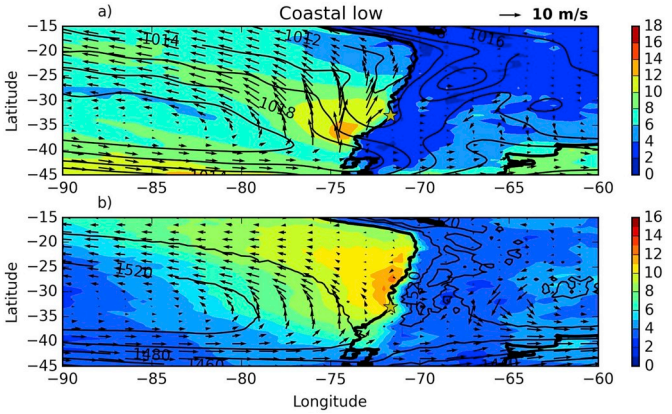

Fig. 2. Composites of a) mean sea level pressure (hPa, solid lines), and wind speed (ms^{-1}, shaded colors) and wind vectors at 1000 hPa and stability parameter x 10^2 (shaded colors) at 850 hPa and b) geopotential height (m, solid lines), relative vorticity stability parameter x 10^2 (KhPa^{-1}, shaded colors) and wind vectors at 850 hPa for the coastal low synoptic situation. The star shows the location of the research site in Valparaiso. (For interpretation of the references to color in this figure legend, the reader is referred to the Web version of this article.)

Composite maps for days with high eBC concentrations for the ***Coastal low*** case (Fig. 2) describe the conditions before the arrival of the coastal low to Valparaíso, characterized by weak winds from the east-northeast due to the associated circulation (Fig. 2a). Relatively low mean sea level pressure values (< 1014 hPa) and a weak surface pressure gradient are observed in the region near the surface, the latter favoring a weak synoptic forcing over the city. The static stability parameter calculated at 850 hPa (Fig. 2b) shows the largest values in the oceanic region where the coastal low is located. When the coastal low approaches the city, its clockwise circulation favors the advection of air masses from the East, which are compressed and warmed adiabatically as they descend from the Andes to the coast. This process may be related to the strengthening of the subsidence inversion along the coast as the coastal low develops, mentioned by Garreaud et al. (2002).

Large values of the stability parameter are also present over the coast of central Chile and further south, indicating the predominance of

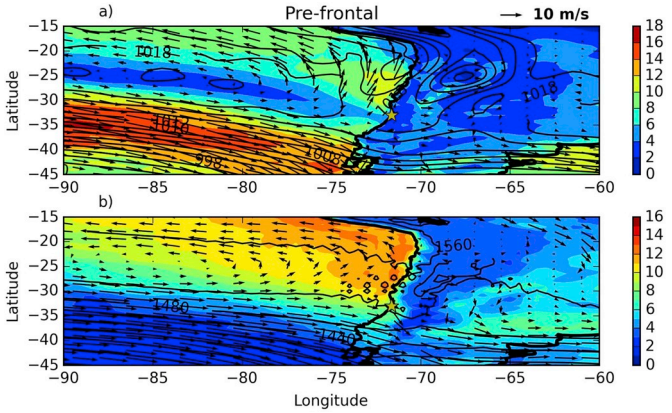

Fig. 3. Same as Fig. 2 but for the pre-frontal synoptic situation.

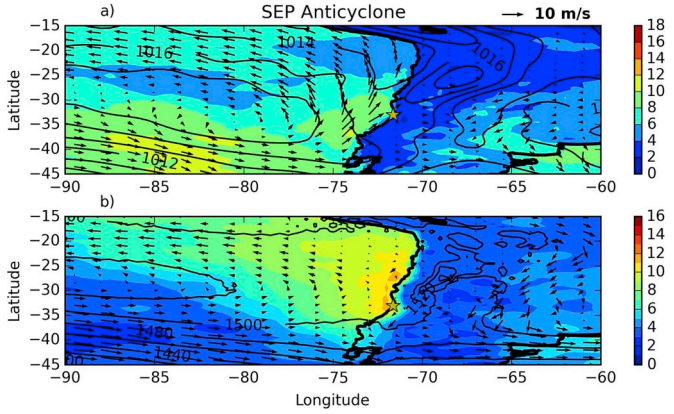

Fig. 4. Same as Fig. 2 but for the SEP anticyclone synoptic situation.

stable conditions. This is also accentuated by the predominance of ridging conditions with westerly winds at mid-levels over the region (Fig. S3b). These synoptic scale features, which have been reported to favor the increase of pollution levels in Santiago, also lead to poor air quality in Valparaiso.

Note that the largest values of eBC for the Coastal low cases are observed on 13 and 15 March 2015. The city of Valparaiso was flooded those two days by the smoke plumes of active fires in the nearby hills and thus, those days are not fully representative of pollution emitted by the typical sources.

Composite maps for days with high eBC concentrations associated with the retreat northwards of the coastal low due to the arrival of a cold front from the south (***Pre-frontal*** case) showed almost large-scale calm over Valparaíso (Fig. 3a) and higher mean surface pressure ($>$ 1018 hPa) than in the ***Coastal low*** case. The static stability parameter calculated at 850 hPa shows smaller values in the city and the oceanic surrounding region than in the ***Coastal low*** case (Fig. 3b), indicating reduced synoptic-scale stability in the lower atmosphere during this case. At mid-levels (not shown), the flow is characterized by intense westerly winds associated with a mid-level ridge. This other synoptic pattern has been associated with a deterioration in air quality in Santiago and also similarly impacts air quality in Valparaiso.

Composite maps for days with high eBC concentrations for the ***SEP anticyclone*** case show weak westerly-southwesterly winds over Valparaíso associated with a low gradient of the surface pressure (Fig. 4a). Mean sea level pressures in the region are higher on average than those in the ***Coastal low*** case but lower than in the ***Pre-frontal*** case. Similar stable conditions seem to be present at low levels as in the **Coastal low** case (Fig. 4b). Westerly-to-west-northwesterly winds predominate at mid-levels (not shown) associated with the leading edge of a mid-level trough. The average eBC value on 29 July 2014 (**SEP anticyclone** case) is larger than that at 13 August 2014, which is the **Coastal low** case that will be studied in detail below. Note that we did not chose 29 July as a case study since eBC values during SEP anticyclone cases are in general lower than those during **Coastal low** and **Pre-frontal** cases. The anomalously large value shown that day is related to not only to the influence of the **SEP anticyclone** but is a day in a transition from the **SEP anticyclone** to the **Pre-frontal** synoptic situation.

The weak synoptic forcing and large-scale stability over Valparaíso during these synoptic situations favor the accumulation of pollution and poor ventilation in the city, contributing to the observed high eBC concentrations and poor air quality in the city. A detailed analysis of the local and/or regional circulations during two high eBC concentration episodes (a ***Coastal low*** and a ***Pre-frontal*** case) is described below in order to study their influence on the advection of pollution to the research site.

5.2. Case studies

In this section, we highlight specific measurements made at the research site during two days when maximum eBC concentrations were observed: 13 August 2014 corresponding to a ***Coastal low*** case and 31 July 2014 corresponding to a ***Pre-frontal*** case. We selected the days that show the largest values of eBC (not associated with forest fires) among the coastal low and pre-frontal cases. We will also analyze the synoptic conditions that favor these highly polluted episodes and determine whether pollution comes from local or regional sources, aided by WRF numerical simulations and back-trajectories with the Hysplit model (Draxler and Hess, 1998; Draxler, 1999; Stein et al., 2015).

5.2.1. Coastal low case: 13 August 2014

The temporal evolution of local meteorological conditions and particle pollution from 00 LT on 12 August to 00 LT on 15 August 2014 is shown in Fig. 6. A large increase in the $PM_{2.5}$ measured at the SINCA station in downtown Valparaiso and the $PM_{2.5}$ derived from measurements at the research site is observed during 13 August 2014 (Fig. 5a), with eBC concentrations reaching values $>$ 13 $\mu g\, m^{-3}$. Note the good agreement between the $PM_{2.5}$ measurements in the city and at the research site, suggestive of a city-wide situation, particularly during 13 August when eBC concentrations increase. Kavouras et al. (2001) analyzed PM_{10} and $PM_{2.5}$ in five cities, including Valparaiso. They reported for Valparaiso mean annual concentrations of 77.5 $\mp$ 2.7 μgm^{-3} and 35.7 $\mp$ 1.8 μgm^{-3} for PM_{10} and $PM_{2.5}$, respectively (see Table 1 in Kavouras et al., 2001). The analysis of $PM_{2.5}$ from the SINCA station in Valparaiso during five years (2013–2017, not shown) shows the highest values during winter months and the lowest values occurring during summer, a similar seasonal evolution as reported for Santiago and other cities in Chile (Yañez et al., 2017). These results do not agree with those reported in Marín et al. (2017). The measurements made close to the port at the VAMPIRE site, indicate elevated $PM_{2.5}$ (and eBC) concentrations also in March (a period of very intense port activities), which are not shown in the SINCA data.

Temperature increased to values larger than 21 °C and the relative humidity (RH) decreased below 30% (Fig. 5b), indicating very dry and warm conditions not generally associated with an austral winter day. The WRF model represents well the temporal evolution of the near-surface temperature and humidity at the field site but largely overestimates temperature and underestimates humidity over the 3-day period (Figs. S2 a, b), showing large errors (Table S1). Low wind speeds ($<$ 2.5 ms^{-1}) from the ESE, uphill from the port (see Fig. 1a), were observed during the high eBC episode (Fig. 5a, c), while the ceilometer indicated a shallow aerosol layer ($<$ 500m) above the research site (Fig. 5d). The PBL height estimated from ceilometer measurements (black stars in Fig. 5d) is below 200 m in the early morning and then increases during the day and the afternoon to a maximum altitude

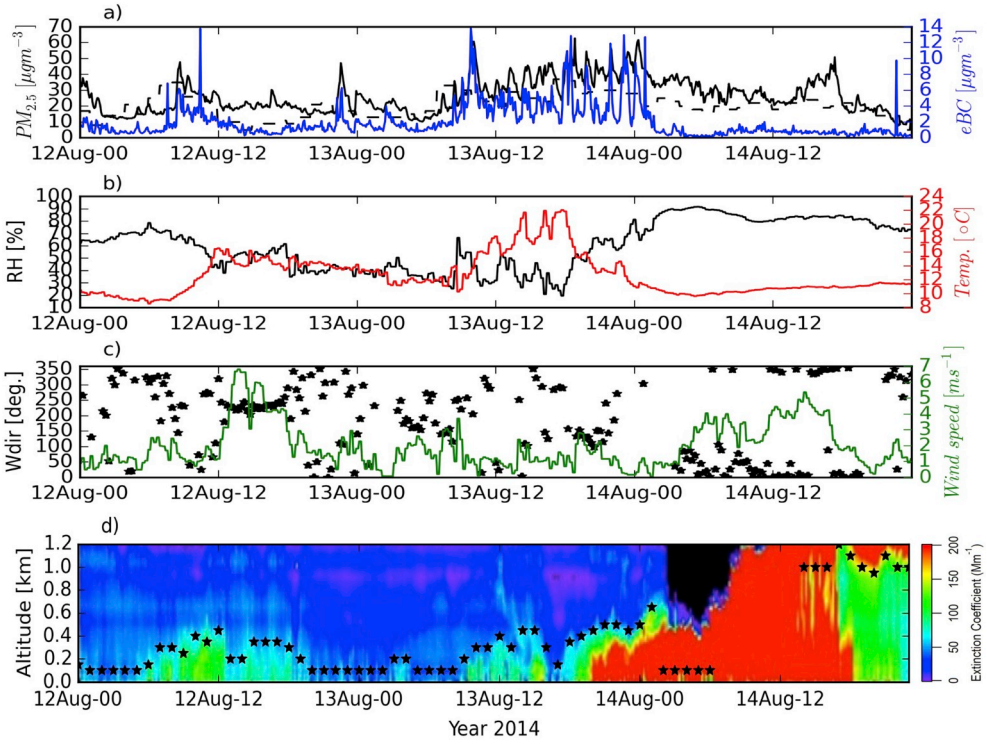

Fig. 5. Temporal evolution (in LT) of a) eBC (blue line) and $PM_{2.5}$ at the research site (solid black line) and $PM_{2.5}$ from SINCA station in Valparaiso (dashed black line), b) temperature and RH, c) wind speed and direction and d) extinction coefficient ($10^6\,m^{-1}$) and PBL heights (black stars) estimated from the ceilometer, at the field site for the period 12 August to 15 August 2014. Curves are shown at 5-min averages, except hourly PBL heights from the ceilometer and $PM_{2.5}$ values from SINCA station in Valparaiso. Wind direction values for wind speeds < 1 m/s were removed from the plot. (For interpretation of the references to color in this figure legend, the reader is referred to the Web version of this article.)

lower than 500 m. The layer of aerosols trapped in a shallow boundary layer due to the poor synoptic ventilation may have caused the increase in pollution at the site. The large values of the extinction coefficient (in red, Fig. 5d) seen during late 13 August indicate the presence of fog over the research site throughout the night. As the denser stratus/stratocumulus cloud moves over the research site, the ceilometer will then determine the cloud-base (as was originally designed for) and no longer will be able to determine the boundary layer height. Note that the boundary layer height (indicated by black stars) show a sudden change during the late morning of 14 August and there is total attenuation of the laser beam at higher altitudes due to the presence of denser clouds.

The cloudiness observed in the satellite image (Fig. 6a) relates to the atmospheric conditions on 13 August 2014 at 18 UTC (14 LT) before the arrival of the coastal low in Valparaiso, where the associated field of low stratocumulus clouds is seen north of the city. Note that clear-sky conditions predominate in parts of central Chile and the adjacent ocean as a result of the influence of the SEP anticyclone and coastal low circulations and the large synoptic scale static stability. The radiosonde launched from Santo Domingo on 14 August 2014 at 00 UTC (13 August at 20 LT) shows a PBL height lower than 700 m with dry and stable conditions from the top of the PBL to mid-levels (Fig. 7a).

Large-scale, near-surface wind speeds that day are relatively high in the oceanic region offshore central Chile at 18 UTC at the boundary between the SEP Anticyclone and the coastal low circulations. However, much lower wind speeds predominate in the city and the inland surrounding areas as shown in Fig. 8a. A wide swath of low wind speeds collocated at the center of the SEP anticyclone has been displaced south around 42°S due to the coastal low southward displacement. Relatively large values of the static stability parameter at 850 hPa are shown in the ocean and along the central Chilean coast that day (Fig. 8b). Garreaud et al. (2002) concludes that the atmospheric stability associated with the SEP anticyclone circulation is reinforced by the circulation associated with the coastal low, whose minimum is located northwest of Valparaiso at 18 UTC, bringing warm, adiabatically-compressed subsiding air from the East (Fig. 8a). In addition, a mid-level ridge is located over the region (Fig. S3), favoring an increase in stability, enhancing the temperature inversion and lowering the PBL height over Valparaíso.

Fig. 9a shows the diurnal evolution of the PBL heights estimated from the ceilometer located at the VAMPIRE site and from the WRF simulation at the nearest grid-point to the research site (only 236 m away) and to the Santo Domingo radiosonde station (582 m away) for three consecutive days (12–14 August 2014). In addition, PBL heights

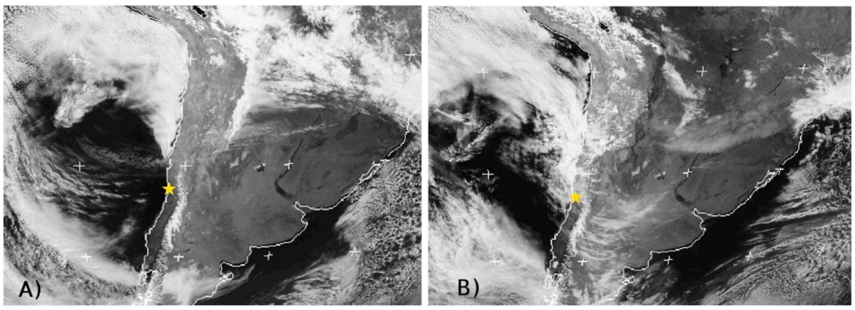

Fig. 6. GOES visible images for a) 13 August 2014 at 18 UTC and b) 14 August 2014 at 18 UTC. Images downloaded from the site: http://www.sat.dundee.ac.uk/.

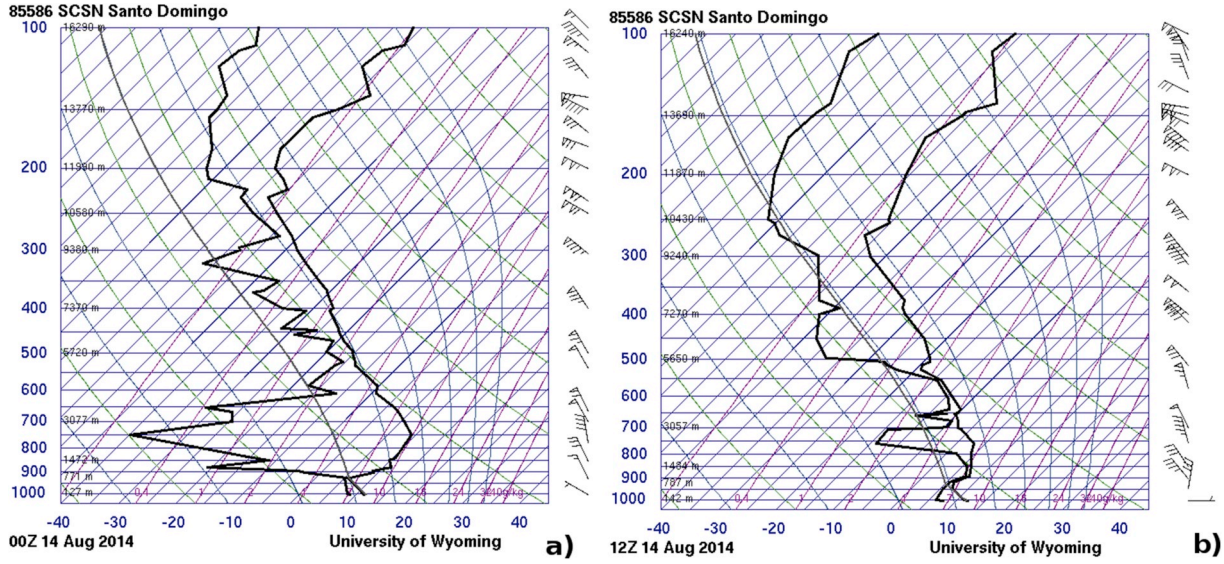

Fig. 7. Skew-T diagrams from radiosondes launched at Santo Domingo station (33.65S, 71.61W) on a) 14 August 2014 at 00 UTC and b) 14 August 2014 at 12 UTC, downloaded from the webpage: http://weather.uwyo.edu/upperair/sounding.html.

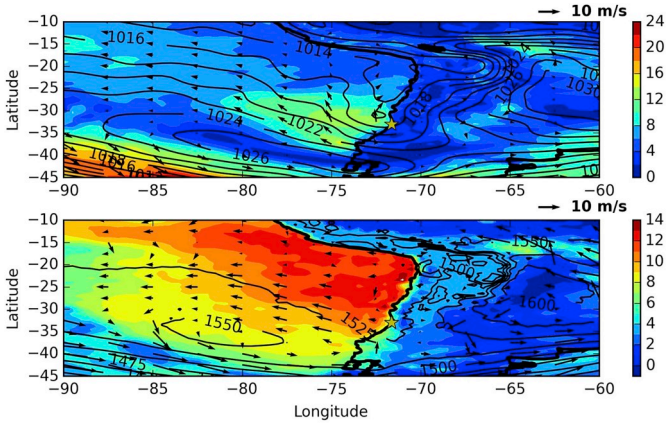

Fig. 8. Horizontal planes of a) sea level pressure (hPa, solid contours), wind direction (arrows) and wind speed (ms^{-1}, shaded colors) at 1000 hPa and b) geopotential height (m, solid contours), and wind vectors at 500 hPa and the static stability parameter at 850 hPa ($KhPa^{-1}$, shaded color) on 13 August 2014 at 18 UTC (14 LT). Yellow stars show the location of Valparaiso. (For interpretation of the references to color in this figure legend, the reader is referred to the Web version of this article.)

estimated from two radiosondes launched at Santo Domingo on 13 and 14 August at 20 LT are also included in the figure.

The observed PBL height from the ceilometer showed a clear diurnal evolution during 12 and 13 August 2014, varying from an altitude lower than 200 m during the night and early morning to an altitude close to 500 m during the day and afternoon hours. The PBL height estimated by the WRF model at the field site represents the observed PBL evolution reasonably well those days, except during the early hours of 12 August, when it largely overestimates it and at the end of 13 August. However, it is important to note that in the first hours of 12 August, the ceilometer shows several layers, possibly from clouds, which makes the estimation of the PBL height difficult. In fact, one of the layers was close to 400 m, the height estimated by WRF for the top of the PBL.

The PBL height during the morning of 13 August is a bit lower than in previous days, favoring the observed increase of $PM_{2.5}$ and eBC at the research site before 12 LT. Note that the model represents very well the evolution of the PBL height during those hours of maximum levels of pollution. On 13 August at 18 LT, the observed PBL height increases and a diurnal cycle seems to occur on 14 August at a higher altitude than in previous days. The increase in PBL height from 18 UTC on 13 August to the end of 14 August is due to the arrival of the cloudiness associated with the coastal low, as it is evident in the GOES satellite visible image that day at 14 LT (Fig. 6b) and the ceilometer backscatter profiles (Fig. 5d). The large discrepancy between the PBL height estimated at the research site and at Santo Domingo may be related with the coastal low closer to Valparaiso than to Santo Domingo, resulting in a higher PBL height at the research site. The PBL parameterization in the WRF model represents a PBL diurnal cycle on 14 August but fails to show the increase in its height that day.

Marín et al. (2017) identified the dominant emission sources of BC in August as diesel-fueled vehicles and wood-burning used for residential heating. Those two sources have a clear diurnal pattern: i) morning rush hour between 07 and 10 LT, preceded by residential wood-burning in the wintertime, and ii) evening rush hour slightly ahead of the increased residential wood-burning emissions.

On average during August, winds at the research site exhibited a clear diurnal pattern, changing direction from south to north between 00 and 12 LT and then changing back to south from 12 to 24 LT. Moreover, maximum values of eBC in August were related to winds flowing from the SSE-SE on average (see Figs. 3b and 11c in Marín et al., 2017). On 13 August 2014, weak wind speeds ($< 2.5\ ms^{-1}$) were observed during most of the day (Fig. 5c). The 10m wind vectors from WRF simulations flowed mostly from the S-SSE downhill to the research site and nearby inland areas during the morning (Fig. 10a). At 09 LT, the local terrain-sea circulation merges with the synoptic forcing from the coastal low and SEP anticyclone circulations. However, at that time, wind vectors and positive vertical velocities indicate an incipient sea breeze circulation going uphill on the western side of the bay, where the research site is located, which converges with the terrain-sea circulation. This line of convergence between the synoptic-scale downhill flow and the mesoscale sea breeze circulation persists until late in the afternoon around the bay (Fig. 10b). Furthermore, during the day, the convergence line moves closer to and even higher on the hill than the research site, likely contributing to the low wind speed values observed.

The WRF model was able to reproduce the mesoscale sea-breeze circulation around the bay that day, as well as its interaction with the synoptic-scale circulations. The large increase in $PM_{2.5}$ and eBC during daytime on 13 August may be due to the advection of pollution by the sea-breeze circulation from the city/port uphill to the research site. A

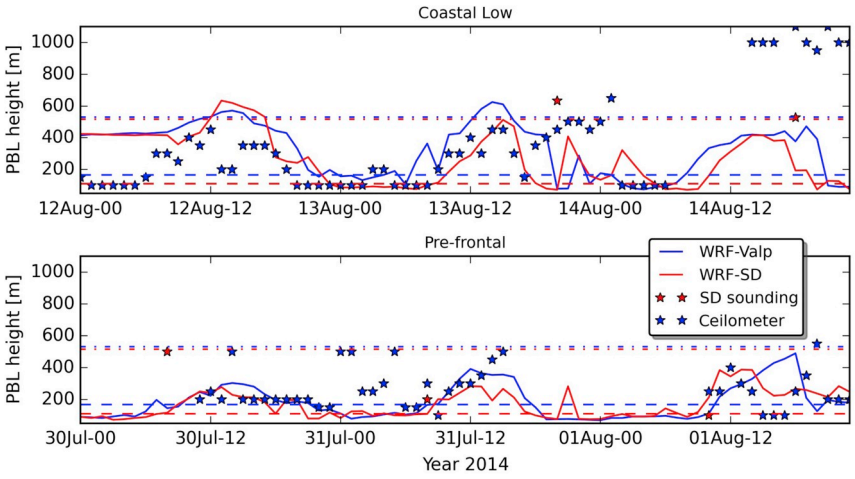

Fig. 9. Temporal evolution (in LT) of PBL height estimated from the ceilometer installed at the research site (blue stars), from radiosondes launched on the 3-day periods (red stars) and from WRF simulations at the nearest grid-point to the field site and to the radiosonde launching site (Santo Domingo, SD) for a) the coastal low (12–14 August 2014), and b) pre-frontal (30 July - 1 August 2014) cases. Dashed (dashed-dotted) blue and red lines represent the mean daily minimum (maximum) PBL heights from 25 July to 31 August 2014 at the VAMPIRE site and Santo Domingo, respectively. See the legend for details. (For interpretation of the references to color in this figure legend, the reader is referred to the Web version of this article.)

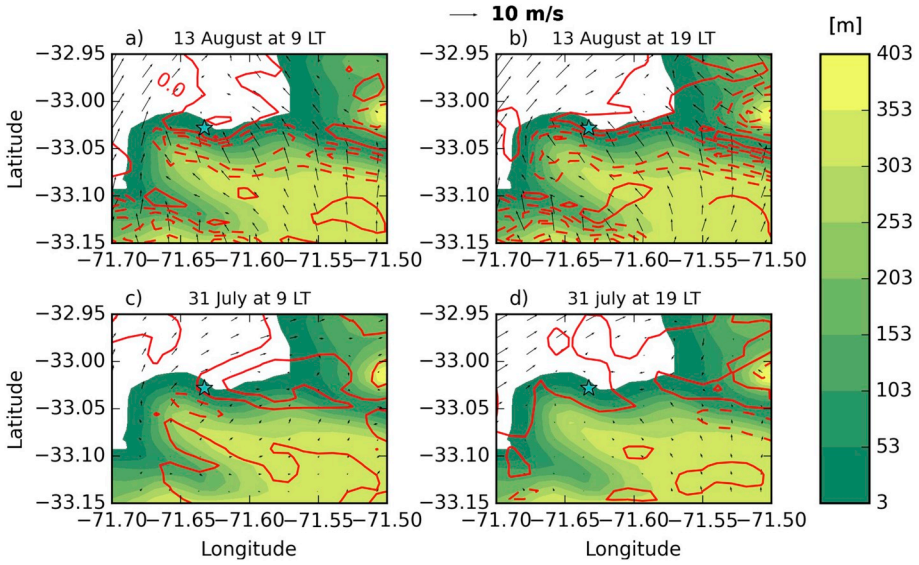

Fig. 10. Horizontal cross sections of 10m wind vectors and vertical velocity (ms^{-1}) showing positive values (solid lines) and negative values (dashed lines) at intervals of 0.2 ms^{-1}, for 13 August 2014 (coastal low case) at a) 9 LT and b) 19 LT and for 31 July 2014 (pre-frontal case) at c) 9 LT and d) 19 LT. The cyan star shows the location of the research site in Valparaiso. Shaded colors show the terrain height in meters. (For interpretation of the references to color in this figure legend, the reader is referred to the Web version of this article.)

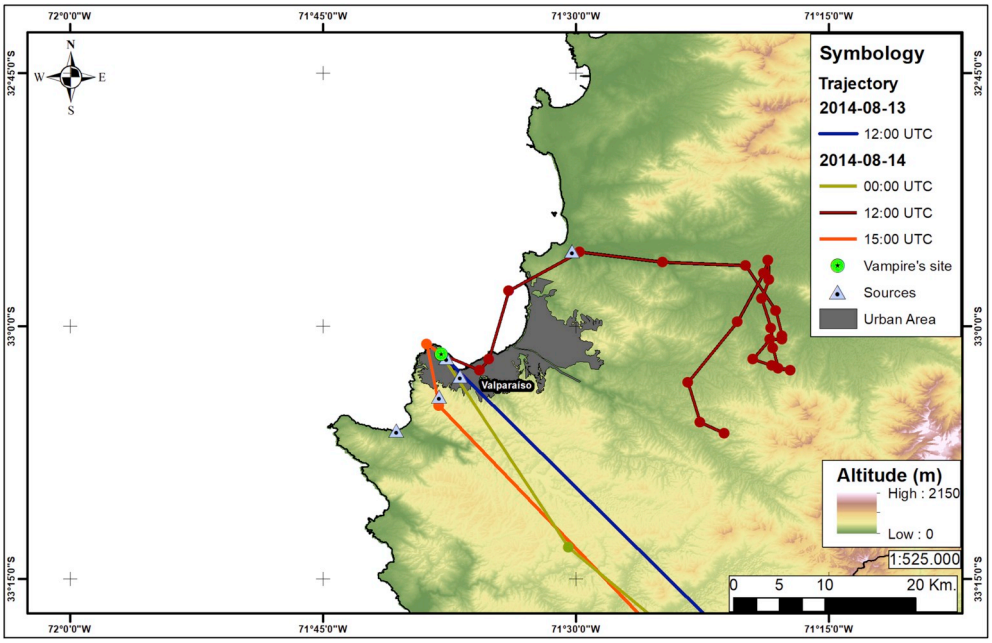

Fig. 11. Back-trajectories calculated with the Hysplit starting on 13 August 2014 at 08 and 20 LT and 14 August 2014 at 08 and 11 LT.

number of studies in other parts of the world have shown how the sea-breeze or lake-breeze circulations can transport pollution, affecting urban air quality, with the strength of the circulation and its inland penetration being particularly important (Harris and Kotamarthi, 2005; Talbot et al., 2007; Brooks et al., 2013).

A large sheet of low stratocumulus clouds, detected in the radiosonde profile and satellite imagery, characterizes the trailing region of the coastal low. The arrival of this cloudiness in Valparaiso on 14 August (clearly evident in the visible GOES image at 18 UTC, Fig. 7b) provides a removal mechanism for the particle pollution via wet scavenging, as evidenced by the rapid decrease in eBC concentrations that day (Fig. 5a). Low and middle clouds are observed in the Santo Domingo radiosonde profile, launched on 14 August at 12 UTC (Fig. 7b), and are also indicated by the ceilometer at the research site (Fig. 5d). In addition, colder temperatures, larger RH values and winds flowing from the North, associated with the cyclonic circulation of the surface coastal low, were recorded most of the day at the field site. The WRF model shows the northerly change of the winds at the site but it underestimates its magnitude (Fig. S2d).

Output from the WRF simulations were used to calculate backward trajectories using the Hysplit model, initiating at 08 and 20 LT at the research site on 13 August. The trajectories illustrate the arrival of continental air masses at the research site at those times (Fig. 11), indicating the stronger influence of the terrain-sea + synoptic circulations associated with the SEP anticyclone and the coastal low. Continental air masses continued from the S-SE on 14 August at 08 LT but the air masses were arriving at the research site after going over the city and the port, located directly to the east of the research site. This synoptic forcing from the east was probably associated with the circulation of the coastal low, with subsiding dry and warm air from the mountains. On 11 LT on 14 August the air masses arrive to the site from the N-NW after going down from the hill, indicating the larger influence of the sea-breeze circulation at that time of the day.

Rutllant and Garreaud (1995) identify the arrival of the coastal low as the most frequent synoptic pattern associated with pollution events in Santiago. Observed $PM_{2.5}$ values from two SINCA stations in Santiago (Parque O'Higgins and Las Condes) were compared with $PM_{2.5}$ values at Valparaiso to put the latter observations in context (Fig. 12). Note that while the $PM_{2.5}$ diurnal cycle at Parque O'Higgins (located in downtown Santiago) and in Valparaiso coincide in time, concentrations were substantially lower in Valparaiso during 13 August (Fig. 12a). On the other hand, $PM_{2.5}$ values at Las Condes, located at a higher elevation closer to the Andes, were lower than those in Valparaiso that day. This comparison highlights the importance of the measurements made during the VAMPIRE field campaign, which demonstrate the high pollution levels in the coastal city of Valparaiso. The observed synoptic-scale conditions on 13 August favored high concentrations of pollution in central Chile both at the coast and in the central valley where Santiago is located. However, the much larger $PM_{2.5}$ concentrations observed in downtown Santiago are related to its geographical location in a valley surrounded by mountains that inhibit ventilation.

In summary, it is clear from the low PBL heights shown by the observations (ceilometer and radiosonde profiles) and the WRF simulation, along with the weak wind and the predominant wind direction during maximum eBC concentrations on 13 August, that these were all favorable conditions for high levels of pollution in Valparaiso as observed. The low wind speeds observed that day were likely the result of the interaction between the synoptic-scale circulation favoring downhill flow and the local uphill sea breeze. As a result, a convergence line forms higher up on the hill, close to the research site, favoring the arrival of polluted air masses from the port and/or the city. The arrival of the coastal low on 14 August, with its circulation and associated cloudiness, led to the observed eBC decrease at the research site.

5.2.2. Pre-frontal case: 31st July 2014

Valparaiso was under the influence of the surface coastal low on 30 July 2014, as evidenced by the low temperature, large RH (close to 100%) (Fig. 13b) and the strong signal in the backscatter profile (Fig. 13d). The synoptic situation indicated the presence of a cold front approaching the region from the south, which resulted in the coastal low being displaced northward on 31st July 2014, with the associated temperature increase and RH decrease at the research site (Fig. 13b). Very high particle pollution levels were recorded on 31 July, with $PM_{2.5}$ concentration at the research site in Valparaiso exceeding 80 $\mu g\,m^{-3}$ early in the morning and up to 120 $\mu g\,m^{-3}$ around mid-day (Fig. 13a). The $PM_{2.5}$ time series at the research site and the SINCA station in Valparaiso both indicated three peaks on 31 July around 01, 11 and 21 local time (LT). As presented in Marín et al. (2017), the eBC sampled at the research site showed a very good correlation with $PM_{2.5}$ at the SINCA station and on 31 July, the corresponding peaks in eBC around 11 and 21 LT exceeded 15 $\mu g\,m^{-3}$ (Fig. 13a). In order to put these observations in context, the diurnal evolution of mean August 2014 eBC concentration showed only two peaks: one after sunrise during the morning rush hour and another after sunset, linked to early night rush hour and wood-burning for residential heating (Marín et al., 2017). The monthly-mean diurnal cycle is consistent with the eBC peaks observed at 11 and 21 LT on 31 July 2014. Large eBC values at 01 LT were also likely associated with residential wood-burning, which is common in some sectors of the city during nighttime in winter. The analysis of WRF and Hysplit simulations will help to better understand this diurnal trend.

Note that on 30 July, while eBC concentration was very low, much lower than on 31 July, the $PM_{2.5}$ concentration at the research site was large, reaching up to 120 $\mu g\,m^{-3}$. Also note that the site was immersed in fog, with RH very close to 100% for about 12 h, indicated also in the ceilometer data (shallow red color layer from the surface to 200 m). The lack of correlation between eBC and $PM_{2.5}$ during that time is indicative of different particle sources and, given the presence of fog, it is likely that the additional particulate mass may be related to the additional water in the deliquesced particles (since particles were not dried prior to sampling) and/or may be the result of cloud processing through aqueous phase production of sulfate. Since no measurements were made of the chemical composition of $PM_{2.5}$ we acknowledge that this latter statement is somewhat speculative.

A decrease in RH and an increase in temperature are observed at the research site on 31 July (Fig. 13b) as the coastal low retreats to the north. Weak winds ($< 2.5\,ms^{-1}$) were observed throughout the day at the field site, predominantly from the southeast (Fig. 13c). The vertical profile of the extinction coefficient at the research site showed an enhanced layer below 0.7 km from 10 to 12 LT (Fig. 13d, note that ceilometer window became contaminated during the afternoon and evening). The $PM_{2.5}$ and eBC peaks shown at 21 LT (Fig. 13a), suggest the presence of a shallow aerosol layer in the city during the remainder of the day.

When the synoptic-scale distribution of wind speed at 1000 hPa is analyzed for this day, the above-mentioned wide swath of low wind speed values from the central region of the SEP anticyclone, can be seen located over Valparaiso and coastal central Chile (Fig. 14a). Much larger wind speed values are shown over the ocean to the South and North of this region of weak winds. The static stability parameter at 850 hPa shows larger values over the ocean, north of the city, associated with the SEP anticyclone circulation (Fig. 14b). Stability values at 850 hPa over the city are a little lower for this case than for the coastal low case (Fig. 8b). Ridging conditions predominate at mid-levels over the city (Fig. S4b), favoring subsidence and the decrease of the planetary boundary layer height as is shown in Fig. 9b.

The boundary layer height values from 0 to 12 LT from the ceilometer are larger than during the coastal low case, which may have resulted from smaller values of the static stability parameter (at 850 hPa) for this case. PBL heights larger than 500 m within this period of PBL heights below 300 m (0–12 LT) may be due to the presence of clouds over the city because of the approaching cold front. The PBL

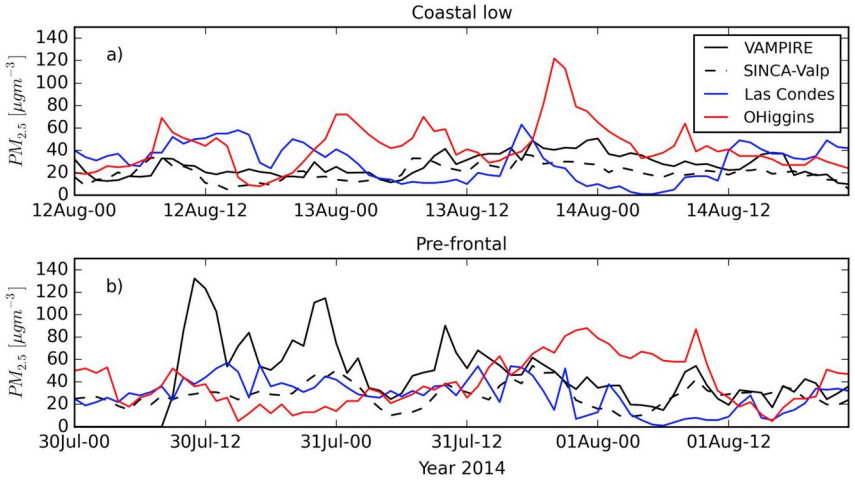

Fig. 12. Temporal evolution of $PM_{2.5}$ observations from SINCA stations in Valparaiso and Santiago (Las Condes and Parque O'Higgins), and $PM_{2.5}$ observations from the research site for a) the coastal low case from 12 to 14 August 2014 and b) the pre-frontal case from 30 July to 1 August 2014.

height estimated from the WRF model at Santo Domingo was in close agreement with the PBL height estimated from radiosondes launched on 31 July and 1 August at 20 LT, indicating a shallow PBL. The agreement was poor on 30 July, with the model largely underestimating the PBL height. The WRF model represents reasonably well the PBL height evolution during the 3-day period at the research site, but it underestimated the PBL height during daytime on 31 July probably as a result of misrepresentations in the cloud field.

The cold front was approaching Valparaiso from the South, and at 09 LT (13 UTC), the synoptic wind forcing was from the SW over the ocean. At the same time, near the research site the land breeze flows downhill to the bay mostly from the SW (Fig. 10c). A local cyclonic circulation appears over the bay at that hour, bringing air masses from the E-ESE to the site, in agreement with the observed S-SSE wind direction observed (Fig. 13c). This circulation is likely the result of the interaction between the synoptic-scale flow with the topography around the bay and the mesoscale sea-land breeze. Note that wind speeds are low all over, aided by a weak synoptic forcing. A backward trajectory calculated with the Hysplit model in 31 July at 08 LT showed that air masses arrive at the research site from the ocean to the SW and downhill to the site in 1 h (Fig. 15). The eBC concentration is lower at that time (< 10 μg/m^{-3}), clear-sky conditions are shown by the ceilometer profiles in the 0–2 km layer (Fig. 13d), and the GOES image showed only high cirrus clouds over the site. The sea breeze from the bay develops at 09 LT and by 11 LT, an intense sea breeze is shown in conjunction with upslope flow that converges at the top of the hills that surround the city.

The eBC concentration started to increase after 08 LT with a peak

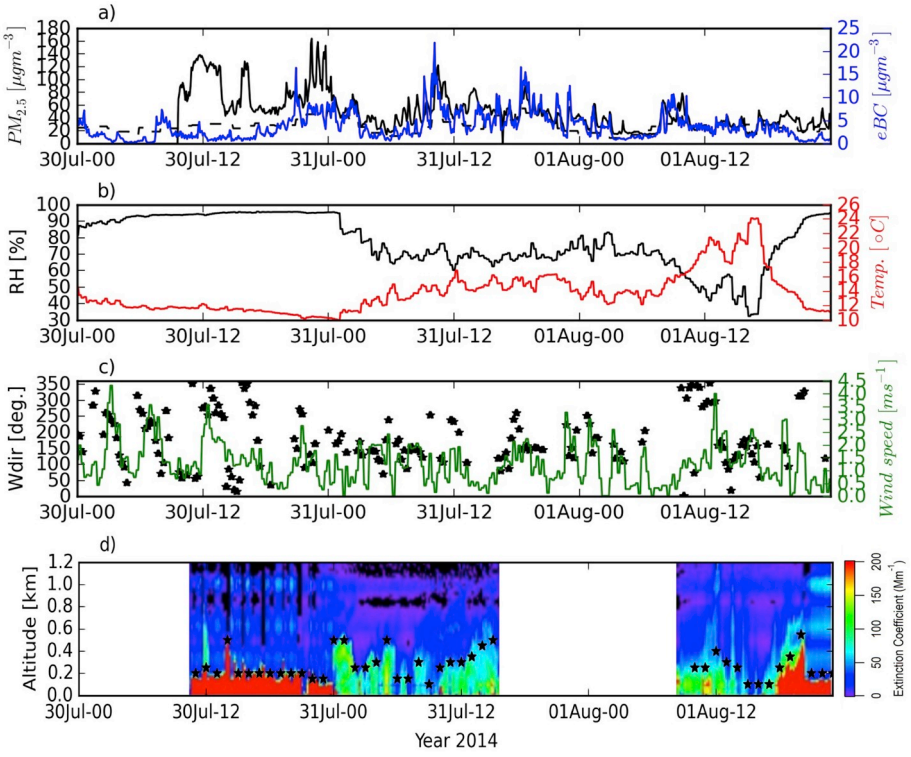

Fig. 13. Same as Fig. 6, but for the pre-frontal case from 30 July to 1 August 2014. White areas in panel d) represent time periods with missing or erroneous ceilometer data.

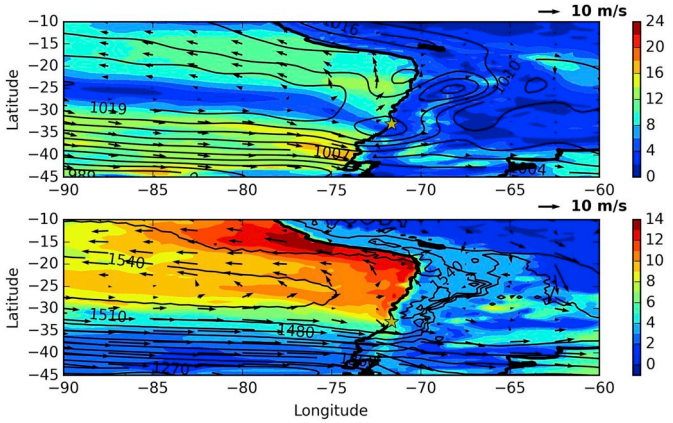

Fig. 14. Same as Fig. 8, but for 31 July at 18 UTC, for the pre-frontal case.

between 10 and 11 LT coincident with the peak seen around that hour in the monthly-mean eBC diurnal evolution (Marín et al., 2017). A Hysplit backward trajectory initiated at 11 LT on 31 July showed that air masses arrived at the site uphill and close to the surface from the East going over the port 3h before. Before that, air masses recirculate over Valparaiso bay likely linked to the cyclonic mesoscale circulation around the bay previously mentioned, related to the land-sea breeze. The $PM_{2.5}$ increased between 10 and 11 LT at the SINCA station in downtown Valparaiso and at the field site (Fig. 13a). High vehicular traffic at and around that time likely caused the increase in $PM_{2.5}$; however, the much larger values observed at the research site were likely mainly related to port emissions advected by the sea breeze that persisted from the morning until late in the afternoon, after the land breeze dominates.

At 19 LT, the cyclonic circulation still persists over the bay (Fig. 10d). The $PM_{2.5}$ from the SINCA station in Valparaiso shows a peak around that time, coinciding with peaks in $PM_{2.5}$ and eBC recorded at the research site, but here the $PM_{2.5}$ is larger than at the SINCA station. The Hysplit backward trajectory initiated at 20 LT from the research site shows air masses coming from the East over the port in agreement with the near-surface wind field in Fig. 13c. The analysis of back-trajectories suggests that advection from local pollution sources such as the port may have contributed to large eBC concentrations observed that day at the research site. Daily maximum values of eBC are likely the result of air masses advected from the bay to the research site by the sea breeze. In addition, the very weak winds observed and the low PBL height -predicted by the model-, inhibited ventilation of pollutants.

The importance of the mesoscale sea-land breeze circulation advecting polluted air to the research site, during a day of weak synoptic forcing in Valparaiso, is highlighted in Fig. 12b. During this day of favorable synoptic conditions for poor air quality in Valparaiso, the $PM_{2.5}$ concentration in downtown Santiago (O'Higgins station) is lower than at the research site between 0 and 14 LT. This highlights that under favorable synoptic-and meso-scale interactions Valparaiso can experience larger concentrations of pollutants than those measured in a megacity like Santiago. Also note that $PM_{2.5}$ concentrations in downtown Santiago continue to increase throughout the day due to large emission sources, reaching close to 100 $\mu g/m^{-3}$ in the evening rush hour.

6. Conclusions

This study discusses the synoptic situations associated with cases of elevated pollution, characterized by high eBC concentrations at the research site during the four months of the VAMPIRE project. Cases in which the concentration of eBC exceeded the 85th percentile were selected to assemble composite synoptic situations, resulting in a total of fifteen cases analyzed. These fifteen cases occurred during one of the three prevalent synoptic situations identified and labeled as:

i) ***Coastal low*** characterized by weak east-northeasterly wind and very low PBL height due to an enhancement of the temperature

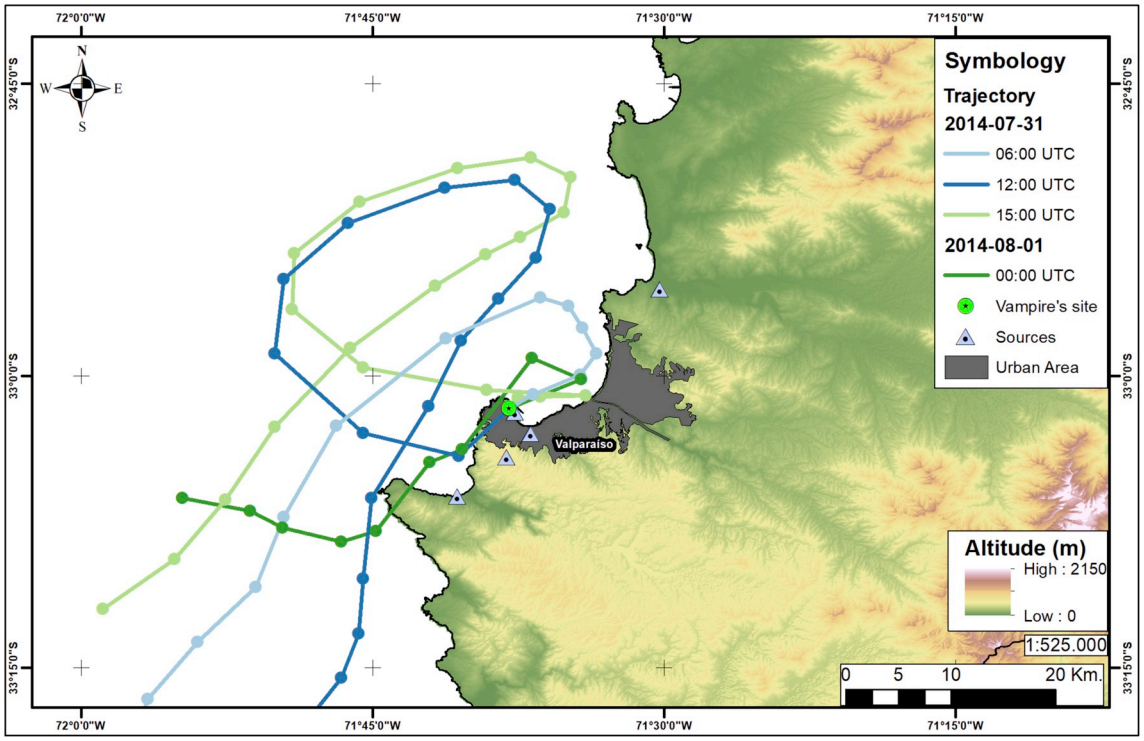

Fig. 15. Back-trajectories calculated with the Hysplit model starting on 31st July 2014 at 02, 08, 11 and 21 LT. See legend for details. WRF simulations provide the meteorological input to Hysplit.

inversion before the arrival of the coastal low. Seven ***Coastal low*** cases were observed not only during winter but in all four months of the VAMPIRE field campaign, up to March. Rutllant and Garreaud (1995) identified this situation as the most frequently associated with severe pollution winter episodes in Santiago. The results presented here indicate an association of high pollution events in Valparaiso prior to the arrival of the coastal low not only during winter but also during December, January and March. It highlights for the first time the importance of this meteorological situation in air quality deterioration at the coastal site during summer and early fall, associated with emissions from local sources of pollution.

ii) ***Pre-frontal*** also characterized by low PBL height, with a cold front approaching from the South and the coastal low retreating northwards, associated with high pollution episodes in Santiago (Rutllant and Garreaud, 1995). Three ***Pre-frontal*** cases were observed at the end of July and August 2014, corresponding to the austral winter. The combined sea-level pressure distribution from the cyclonic circulation associated with the approaching cold front, the coastal low and the circulation associated with the SEP anticyclone results in slow and divergent surface winds in the region. Rutllant and Garreaud (1995) identified this pattern as one less frequently associated with pollution episodes in Santiago. This study has confirmed that the situation also leads to high pollution episodes in Valparaiso.

iii) ***SEP anticyclone*** characterized by large stability, very low gradient in the mean sea level pressure and weak westerly-southwesterly wind due to the dominance of the SEP anticyclone. Five ***SEP anticyclone*** cases were predominantly observed during austral summer as should be expected, with one additional case identified in July.

All three synoptic situations are consistent with a reduced synoptic forcing, in which the mesoscale sea-land breeze may become predominant, advecting large pollutant concentrations from local/regional emission sources to the research site.

The high-resolution (1 km) WRF simulations performed as part of the study successfully captured the mesoscale sea-breeze circulation during days under weak synoptic forcing. This allows its use to study the effect of the sea-land breeze circulation in the transport of pollution over coastal cities in Chile and other parts of the world with similar geographical and meteorological characteristics. The WRF model simulated reasonably well the evolution of near-surface meteorological variables in the region during August 2014, and the PBL height during the cases studied. The rmse for temperature ranged between 3.6 and 4.1 °C, between 21.6 and 22.5% for RH and between 1.3 and 2.4 ms^{-1} for both wind components during August 2014. These model errors are somewhat large and are related to the difficulty of simulating regional circulations over complex terrain. New simulations at horizontal resolutions < 1 km should be carried out to improve the model results. However, an elevation terrain model at a similar resolution would be required.

The detailed analysis of two case studies, one ***Coastal low*** (13 August 2014) and one ***Pre-frontal*** (31 July 2014), highlights the interaction between the synoptic-scale meteorological conditions (low PBL height and weak wind speeds) and mesoscale flows advecting polluted air, leading to quite severe cases of pollution in Valparaiso. The results of the high-resolution WRF simulations allow the identification of the particular air-mass trajectories that are associated with the observed peaks of eBC at the research site under each case and also provide support to the relative role of the different sources that contribute to the high pollution values observed. Furthermore, the interplay between the synoptic conditions and the mesoscale circulation identified during VAMPIRE provides evidence and insight that will aid in future air quality forecasts for Valparaiso.

Operational WRF simulations are currently conducted every day by the Chilean Weather Service and by the regional Navy Weather Service. While there are currently no plans for the implementation of an air quality forecast system in Valparaiso, such a system could combine the output from high-resolution WRF simulations supplemented by forward trajectories (e.g. Hysplit). In cases in which the forecast is similar to one of the three synoptic patterns discussed in this study, a series of measures could be devised by policymakers to avoid reaching the high pollution that would ensue if no actions were implemented. Currently, Valparaiso only has one $PM_{2.5}$ monitoring station, which is not sufficient to capture the variability in concentration that is associated with the complex mesoscale circulations and more air quality stations would be necessary for diagnostic as well as for validation purposes.

The study by Yañez et al. (2017) used regression techniques to show that particulate matter in a few, land-locked cities in Chile, is largely related to meteorological variables that could be used as predictors for PM levels. In principle, a similar approach could be applied in Valparaiso, even though the emission sources would not necessarily correspond to the typical urban conditions (e.g. port activities). The observations gathered during the VAMPIRE field campaign could be used to generate a statistical observationally-based forecasting system to predict pollution concentrations in the city. However, this approach would require a larger dataset that the one gathered during VAMPIRE for statistical robustness. Moreover, a larger number of meteorological stations would be needed at different sites for the method to be a reliable predictor of PM under complex topography.

Results from this study show that the mesoscale sea-breeze circulation plays a key role in advecting pollution towards the city during weak synoptic forcing. As other port cities in western South America (e.g. Callao, Perú; Guayaquil, Ecuador) share similar climate and geographic characteristics as Valparaiso, the same processes may also be a major contributing factor in poor air quality in those cities. High-resolution regional simulations with the WRF model would be highly recommended to quantify the role of mesoscale circulations. A number of studies have shown that the future climate is expected to have more frequent episodes of stagnant conditions, due to more frequent high-pressure systems and the decrease in the frequency of mid-latitude cyclonic perturbations, responsible for increasing ventilation (Mickley et al., 2004; Leibensperger et al., 2008; Jacob and Winner, 2009). The synoptic patterns identified in this study are associated with stagnant surface conditions, which could be more frequent in the future, negatively impacting on the air quality of Valparaiso.

Acknowledgments

This study was the result of collaboration between Universidad Autónoma de México (UNAM) and Universidad de Valparaíso under an umbrella agreement. UNAM is gratefully acknowledged for covering the costs of transportation of the equipment from Mexico City to Chile and for support during the fieldwork. JCM acknowledges the projects FONDECYT 11121473 and Conicyt-MEC 80140111 for support. Powered@NLHPC: This research was partially supported by the supercomputing infrastructure of the National Laboratory for High Performing Computer (NLHPC) (ECM-02). The Climate Forecast System v2 was provided by the Research Data Archive at the National Center for Atmospheric Research, Computational and Information Systems Laboratory. The air quality data was obtained from the Chilean government through their Sistema de Información Nacional de Calidad del Aire (SINCA) network. GBR acknowledges the support of PASPA-DGAPA during the 6-month sabbatical at the University of Valparaiso, Chile.

Appendix A. Supplementary data

Supplementary data to this article can be found online at https://doi.org/10.1016/j.atmosenv.2018.10.006.

References

Arnott, W.P., Moosmüller, H., Walker, J.W., 2000. Nitrogen dioxide and Kerosene-Fla.me soot calibration of photoacoustic instruments for measurement of light absorption by aerosols. Rev. Sci. Instrum. 71, 4545–4552.

Barrett, B.S., Hameed, S., 2017. Seasonal variability in precipitation in central and southern Chile: modulation by the south pacific high. J. Clim. 30 (1), 55–69.

Bei, N., Li, G., Molina, L.T., 2012. Uncertainties in SOA simulations due to meteorological uncertainties in Mexico City during MILAGRO-2006 field campaign. Atmos. Chem. Phys. 12, 11295–11308. https://doi.org/10.5194/acp-12-11295-2012.

Bei, N., Li, G., Zavala, M., Barrera, H., Torres, R., Grutter, M., Gutiérrez, W., García, M., Ruiz-Suarez, L.G., Ortinez, A., Guitierrez, Y., Alvarado, C., Flores, I., Molina, L.T., 2013. Meteorological overview and plume transport patterns during CalMex 2010. Atmos. Environ. 70, 477–489.

Bei, N., Li, G., Huang, R.-J., Cao, J., Meng, N., Feng, T., Liu, S., Zhang, T., Zhang, Q., Molina, L., 2016. Typical synoptic situations and their impacts on the wintertime air pollution in the Guanzhong basin, China. Atmos. Chem. Phys. 16, 7373–7387 2016.

Bond, T.C., Doherty, S.J., Fahey, D.W., Forster, P.M., Berntsen, T., DeAngelo, B.J., Flanner, M.G., Ghan, S., Karcher, B., Koch, D., Kinne, S., Kondo, Y., Quinn, P.K., Sarofim, M.C., Schultz, M.G., Schulz, M., Venkataraman, C., Zhang, H., Zhang, S., Bellouin, N., Guttikunda, S.K., Hopke, P.K., Jacobson, M.Z., Kaiser, J.W., Klimont, Z., Lohmann, U., Schwarz, J.P., Shindell, D., Storelvmo, T., Warren, S.G., Zender, C.S., 2013. Bounding the role of black carbon in the climate system: a scientific assessment. J. Geophys. Res. 118, 5380–5552.

Bretherton, C.S., Uttal, T., Fairall, C.W., Yuter, S.E., Weller, R.A., Baumgardner, D., Comstock, K., Wood, R., Raga, G.B., 2004. The EPIC2001 stratocumulus study. Bull. Am. Meteorol. Soc. 85, 967–977.

Brooks, J.R., Makar, P.A., Sills, D.M.L., Hayden, K.L., McLaren, R., 2013. Exploring the nature of air quality over southwestern Ontario: main findings from the Border air quality and meteorology study. Amos. Chem. Phys. 13, 10461–10482.

Cheng, W.L., Pai, J.L., Tsuang, B.J., Chen, C.L., 2001. Synoptic patterns in relation to ozone concentrations in West-Central Taiwan. Meteorol. Atmos. Phys. 78 (11–21).

Comstock, K.K., Bretherton, C.S., Yuter, S.E., 2005. Mesoscale variability and drizzle in southeast Pacific stratocumulus. J. Atmos. Sci. 62, 3792–3807.

Córdova, A.M., Arévalo, J., Marín, J.C., Baumgardner, D., Raga, G.B., Pozo, D., Ochoa, C.A., Rondanelli, R., 2016. On the transport of urban pollution in an Andean mountain valley. Aerosol and Air Quality Research 16, 593–605.

Crawford, J., Griffiths, A., Cohen, D.D., Jiang, N., Stelcer, E., 2016. Particulate pollution in the Sydney region: source diagnostics and synoptic controls. Aerosol and Air Quality Research 16, 1055–1066.

Cuchiara, G.C., Rappenglück, B., Rubio, M.A., Lissi, E., Gramsch, E., Garreaud, R.D., 2017. Modeling study of biomass burning plumes and their impact on urban air quality; a case study of Santiago de Chile. Atmos. Environ. 166, 79–91. https://doi.org/10.1016/j.atmosenv.2017.07.002.

Davis, R.E., Kalkstein, L.S., 1990. Using a spatial synoptic climatological classification to assess changes in atmospheric pollution concentrations. Phys. Geogr. 11, 320–342.

Draxler, R.R., 1999. HYSPLIT4 User's Guide. NOAA Tech. Memo. ERL ARL-230. NOAA Air Resources Laboratory, Silver Spring, MD.

Draxler, R.R., Hess, G.D., 1998. An overview of the HYSPLIT_4 modeling system of trajectories, dispersion, and deposition. Aust. Meteorol. Mag. 47, 295–308.

Eastman, J.L., Pielke, R.A., Lyons, W.A., 1995. Comparison of lake-breeze model simulations with tracer data. J. Appl. Meteorol. 34, 1398–1418.

García-Franco, J.L., Stremme, W., Bezanilla, A., Ruiz-Angulo, A., Grutter, M., 2018. Variability of the mixed-layer height over Mexico City. Boundary-Layer Meteorol. 167, 493–507. https://doi.org/10.1007/s10546-018-0334-x.

Garreaud, R., Rutllant, J., Fuenzalida, H., 2002. Coastal lows along the subtropical west coast of South America: mean structure and evolution. Mon. Weather Rev. 130, 75–88.

Garreaud, R., Rutllant, J., 2006. Factores meteorológicos de la contaminación atmosférica en Santiago. Contaminación atmosférica urbana: episodios críticos de contaminación ambiental en la ciudad de Santiago, Santiago, pp. 36–53.

Grahame, T.J., Klemm, R., Schlesinger, R.B., 2014. Public health and components of particulate matter: the changing assessment of black carbon. J. Air Waste Manag. 64 (6), 620–660.

Gramsch, E., Caceres, D., Oyola, P., Reyes, F., Vázquez, Y., Rubio, M., Sánchez, G., 2014. Influence of surface and subsidence thermal inversion on PM 2.5 and black carbon concentration. Atmos. Environ. 98, 290–298.

Hamburger, T., coauthors, 2011. Overview of the synoptic and pollution situation over Europe during the EUCAARI-LONGREX field campaign. Atmos. Chem. Phys. 11, 1065–1082.

Hannay, C., Williamson, D.L., Hack, J.J., Kiehl, J.T., Olson, J.G., Klein, S.A., Bretherton, C.S., Köhler, M., 2009. Evaluation of forecasted southeast Pacific stratocumulus in the NCAR, GFDL, and ECMWF Models. J. Clim. 22, 2871–2889.

Harris, L., Kotamarthi, V.R., 2005. The characteristics of the Chicago lake breeze and its effects on trace particle transport: results from an episodic event simulation. J. Appl. Meteorol. 44, 1637–1654.

Hidy, G.M., Mueller, P.K., Tong, E.Y., 1978. Spatial and temporal distributions of airborne sulfate in parts of the United States. Atmos. Environ. 12, 735–752.

Hoek, G., Krishnan, M.K., Beelen, R., et al., 2013. Long-term air pollution exposure and cardio-respiratory mortality. Environ. Health 12, 43 2013.

Huneeus, N., Mazzeo, A., Ordóñez, C., Donoso, N., Gallardo, L., Molina, L., Moreno, V., Muñoz, R., Orfanoz, A., Vizcarra, A., 2016. Transport of Particle Pollution into the Maipo Valley: Winter 2015 Campaign Results. EGU General Assembly, Vienna, Austria, pp. 9617 2016, 17-22 April.

Jacob, D.J., Winner, D.A., 2009. Effect of climate change on air quality. Atmos. Environ. 43 (1), 51–63.

Janssen, N.A.H., Hoek, G., Simic-Lawson, M., Fischer, P., van Bree, L., ten Brink, H., Keuken, M., Atkinson, R.W., Anderson, H.R., Brunekreef, B., Cassee1, F.R., 2011. Black carbon as an additional indicator of the Adverse health effects of airborne particles compared with PM10 and PM2.5. Environ. Health Perspect. 119 (12), 1691–1699.

Janssen, N.A., Gerlofs-Nijland, M.E., Lanki, T., Salonen, R.O., Cassee, F., et al., 2012. Health Effects of Black Carbon. World Health Organization, Regional Office for Europe Technical report.

Jiang, Y., Liu, X., Yang, X.Q., Wang, M., 2013. A numerical study of the effect of different aerosol types on East Asian summer clouds and precipitation. Atmos. Environ. 70, 51–63.

Jiang, N., Scorgie, Y., Hart, M., Riley, M.L., Crawford, J., Beggs, P.J., Edwards, G.C., Chang, L., Salter, D., Virgilio, G.D., 2016. Visualising the relationships between synoptic circulation type and air quality in Sydney, a subtropical coastal-basin environment. Int. J. Climatol. https://doi.org/10.1002/joc.4770.

Kavouras, I.G., Koutrakis, P., Cereceda-Balic, F., Oyola, P., 2001. Source apportionment of PM10 and PM2.5 in five Chilean cities using factor analysis. J. Air Waste Manag 51, 451–464.

Leibensperger, E.M., Mickley, L.J., Jacob, D.J., 2008. Sensitivity of US air quality to mid-latitude cyclone frequency and implications of 1980–2006 climate change. Atmos. Chem. Phys. 8, 7075–7086.

Marín, J.C., Raga, G.B., Arévalo, J., Baumgardner, D., Córdova, A.M., Pozo, D., Calvo, A., Castro, A., Fraile, R., Sorribas, M., 2017. Properties of particulate pollution in the port city of Valparaiso, Chile. Atmos. Environ. 171, 301–316.

Ménégoz, M., Krinner, G., Balkanski, Y., Boucher, O., Cozic, A., Lim, S., Ginot, P., Laj, P., Gallée, H., Wagnon, P., Marinoni, A., 2014. Snow cover sensitivity to black carbon deposition in the Himalayas: from atmospheric and ice core measurements to regional climate simulations. Atmos. Chem. Phys. 14, 4237–4249.

Mickley, L.J., Jacob, D.J., Field, B.D., Rind, D., 2004. Effects of future climate change on regional air pollution episodes in the United States. Geophys. Res. Lett. 31, L24103. https://doi.org/10.1029/2004GL021216. 2004.

Moisan, S., Herrera, R., Clements, A., 2017. A dynamic multiple equation Approach for forecasting PM2.5 pollution in Santiago, Chile. NCER Working Paper Series #117. http://www.ncer.edu.au/papers/.

Montecinos, A., Aceituno, P., 2003. Seasonality of the ENSO-related rainfall variability in Central Chile and associated circulation Anomalies. J. Clim. 16, 281–296.

Münkel, C., Eresmaa, N., Räsänen, J., Karppinen, A., 2007. Retrieval of mixing height and dust concentration with lidar ceilometer. Bound. Lay. Meteorol. 124, 117–128.

Muñoz, R., Undurraga, A., 2010. Daytime mixed layer over the Santiago basin: description of two years of observations with a lidar ceilometer. J. Appl. Meteorol. 49, 1728–1741.

Nakanishi, M., Niino, H., 2004. An improved mellor-yamada level-3 model with condensation physics: its design and verification. Bound.-Layer Meteorol. 112 (1), 1–31.

Nakanishi, M., Niino, H., 2006. An improved Mellor–Yamada level-3 model: its numerical stability and application to a regional prediction of advection fog. Bound.-Layer Meteorol. 119, 397–407.

Nakayama, T., Suzuki, H., Kagamitani, S., Ikeda, Y., Uchiyama, A., Matsumi, Y., 2015. Characterization of a three-wavelength photoacoustic soot spectrometer (PASS-3) and photoacoustic extinctiometer (PAX). J. Meteorol. Soc. Jpn. 93, 285–308. https://doi.org/10.2151/jmsj.2015-016.

Olivares, G., Gallardo, L., Langner, J., Aarhus, B., 2002. Regional dispersion of oxidized sulfur in Central Chile. Atmos. Environ. 36, 3819e3828.

Orfanoz-Cheuquelaf, A.P., Gallardo, L., Huneeus, N., Lambert, F., 2015. High Resolution Simulations of Pollution Vertical Stratification over Santiago and its Transport to the Chilean Andes. Preprints American Geophysical Union, Fall Meeting 2015, A42B-03.

Pizarro, J.G., Montecinos, A., 2000. Cutoff cyclones off the subtropical coast of Chile. In: Preprints Sixth International Conference on Southern Hemisphere Meteorology and Oceanography (AMS). Santiago, pp. 278–279.

Raga, G.B., Baumgardner, D., Ulke, A.G., Torres Brizuela, M.M., Kucienska, B., 2013. The environmental impact of the puyehue-Cordon Caulle 2011 volcanic eruption on Buenos Aires. Nat. Hazards Earth Syst. Sci. 13, 2319–2330. https://doi.org/10.5194/nhess-13-2319-2013.

Ramanathan, V., Carmichael, G., 2008. Global and regional climate changes due to black carbon. Nat. Geosci. 1, 221–227.

Retama, A., Baumgardner, D., Raga, G.B., McMeeking, G.R., Walker, J.W., 2015. Seasonal and diurnal trends in black carbon properties and co-pollutants in Mexico City. Atmos. Chem. Phys. 15, 9693–9709 2015.

Rodwell, M.J., Hoskins, B.J., 2001. Subtropical anticyclones and summer monsoons. J. Climate 14, 3192–3211.

Rutllant, J., Fuenzalida, H., 1991. Synoptic aspects of the central Chile rainfall variability associated with the Southern Oscillation. Int. Journal of Clim. 11, 63–76.

Rutllant, J., Garreaud, R., 1995. Meteorological air pollution potential for Santiago, Chile: towards an objective episode forecasting. Environ. Monit. Assess. 34, 223–244.

Rutllant, J.A., Fuenzalida, H., Aceituno, P., 2003. Climate dynamics along the arid northern coast of Chile: the 1997–1998 Dinámica del Clima de la Región de Antofagasta (DICLIMA) experiment. J. Geophys. Res. 108 (D17), 4538.

Saha, S., Moorthi, S., Wu, X., Wang, J., Nadiga, S., Tripp, P., Behringer, D., Hou, Y., Chuang, H., Iredell, M., Ek, M., Meng, J., Yang, R., Mendez, Peña, van den Dool, H., Zhang, Q., Wang, W., Chen, M., Becker, E., 2014. The NCEP climate forecast system version 2. J. Clim. 27, 2185–2208.

Saide, P.E., Mena-Carrasco, M., Tolvett, S., Hernandez, P., Carmichael, G.R., 2016. Air quality forecasting for winter-time $PM_{2.5}$ episodes occurring in multiple cities in central and southern Chile. J. Geophys. Res. Atmos. 121, 558–575.

Seguel, R.J., Mancilla, C.A., Rondanelli, R., Leiva, M.A., Morales, R.G.E., 2013. Ozone distribution in the lower troposphere over complex terrain in Central Chile. J.

Geophys. Research-Atmosphere 118, 2966e2980.
Skamarock, W.C., Klemp, J.B., Dudhia, J., Gill, D.O., Barker, D.M., Duda, M., Huang, X.Y., Wang, W., Powers, J.G., 2008. A Description of the Advanced Research WRF Version 3. NCAR Technical Note. NCAR/TN–475 + ST.
Stein, A.F., Draxler, R.R., Rolph, G.D., Stunder, B.J.B., Cohen, M.D., Ngan, F., 2015. NOAA's HYSPLIT atmospheric transport and dispersion modeling system. Bull. Am. Meteorol. Soc. 96, 2059–2077.
Talbot, C., Augustin, P., Leroy, C., Willart, V., Delbarre, H., Khomenko, G., 2007. Impact of a sea breeze on the boundary-layer dynamics and the atmospheric stratification in a coastal area of the North Sea. Bound. Layer Meteor. 125 (1), 133–154.
Toro, R., Donoso, C.S., Seguel, R.A., Morales, R.G.E.S., Leiva, M.A.G., 2013. Photochemical ozone pollution in the Valparaiso region, Chile. Air Qual. Atmos. Health 7, 1–11.
Tsaknakis, G., Papayannis, A., Kokkalis, P., Amiridis, V., Kambezidis, H.D., Mamouri, R.E., Georgoussis, G., Avdikos, G., 2011. Inter-comparison of lidar and ceilometer retrievals for aerosol and Planetary Boundary Layer profiling over Athens, Greece. Atmos. Meas. Tech. 4, 1261–1273. https://doi.org/10.5194/amt-4-1261-2011.
Valparaiso emission inventory, 2011. "Estudio diagnóstico. Plan de gestión atmosférica - Región de Valparaíso, Construcción de un inventario de emisiones regional". Final report made by several institutions diagnosing all the emissions in the region of Valparaiso.
van der Kamp, D., McKendry, I., 2010. Diurnal and seasonal trends in convective mixed-layer heights estimated from two years of continuous ceilometer observations in vancouver, BC. Bound. Meteorol. 137, 459–475.
Wang, H., Xu, J., Zhang, M., Yang, Y., Shen, X., Wang, Y., Chen, D., Guo, J., 2014. A study of the meteorological causes of a prolonged and severe haze episode in January 2013 over central eastern China, Atmos. Environ. Times 98, 146–157.
Wei, P., Cheng, S., Li, J., Su, F., 2011. Impact of boundary-layer anticyclonic weather system on regional air quality. Atmos. Environ. 45, 2453–2463.
Wu, M., Wu, D., Fan, Q., Wang, B.M., Li, H.W., Fan, S.J., 2013. Observational studies of the meteorological characteristics associated with poor air quality over the Pearl River Delta in China. Atmos. Chem. Phys. 13, 10755–10766. https://doi.org/10.5194/acp- 13-10755-2013.
Yañez, M.A., Baettig, R., Cornejo, J., Zamudio, F., Guajardo, J., Fica, R., 2017. Urban airborne matter in central and southern Chile: effects of meteorological conditions on fine and coarse particulate matter. Atmos. Environ. 161, 221–234.